Structural Characterization of the "Knitting Pattern" in Polystyrene-*block*-poly(ethylene-*co*-butylene)-*block*-poly(methyl methacrylate) Triblock Copolymers

Ulrike Breiner, Udo Krappe, Edwin L. Thomas,† and Reimund Stadler*

Institut für Organische Chemie der Johannes Gutenberg-Universität Mainz, J. J. Becher Weg 18-20, D-55099 Mainz, Germany

Received October 21, 1996; Revised Manuscript Received September 29, 1997[⊗]

ABSTRACT: In a polystyrene-*block*-polybutadiene-*block*-poly(methyl methacrylate) triblock copolymer (SBM) a morphological transition from a lamellar (*ll*) morphology (with sequence ABCB) to the *knitting pattern* (*kp*) morphology occurs upon hydrogenation of the center PB block. Structural information of the nonhydrogenated and the hydrogenated material is provided from small angle X-ray scattering (SAXS) and transmission electron microscopy (TEM). For the nonhydrogenated SBM sample the SAXS profile correlates well with a simple periodic lamellar structure. The hydrogenated sample forming the *kp* morphology displays a more complex SAXS pattern. From the TEM images of the *knitting pattern* the two-dimensional space group has been determined to be *c*2*mm*. This morphology represents a first example of a planar morphology for which the two sides of the unit cell are unequal (**a** ≠ **b**). The determination of the space group from TEM allows the satisfactory assignment of the SAXS pattern. Furthermore this new *kp* morphology is the first example in block copolymers providing a *highly* nonconstant mean curvature (NCMC) intermaterial dividing surface. Varying the casting solvent for this material (from $CHCl_3$ to toluene) results in a lamellar morphology as demonstrated by TEM and SAXS. This morphological change is explained as the consequence of the borderline situation of the *kp* morphology as an intermediate between the *ll* and *lc* morphology where B cylinders of the center block are located at the lamellar A/C interface.

Introduction

In AB diblock copolymers the morphology is primarily governed by the composition of the block copolymer, expressed by the volume fractions of the components.[1−3] In contrast, microphase separation in ABC triblock copolymers consisting of three different components A, B, and C can result in a greater variety of morphologies, since the formation of microphase-separated assemblies is influenced by two independent composition parameters: ϕ_A, ϕ_B, the volume fractions of components A and B, and the relative incompatibilities, expressed by the interfacial tensions γ_{ij}, between the directly connected blocks A/B, B/C, and the "nonlinked" blocks A/C. Furthermore, the sequence along the chain of the three components can also alter the microstructural arrangement.[4,5] In an earlier study we reported a transition from a lamellar (*ll*) morphology (lamellar sequence: ABCB) to a *lc* morphology (AC lamella with B cylinders at the A/C lamellar interface) in both a symmetric (i.e., $\phi_A = \phi_C$) polystyrene-*block*-polybutadiene-*block*-poly(methyl methacrylate) (SBM) and in a symmetric (i.e., $\phi_A = \phi_C$) polystyrene-*block*-poly(ethylene-*co*-butylene)-*block*-poly(methyl methacrylate) (SEBM) triblock copolymer where polybutadiene (PB) (or poly(ethylene-*co*-butylene) (PEB) respectively) cylinders of the center block were located at the interface between the S/M lamellae.[6] This structural transition occurred upon reduction of the volume fraction of the center block. At the borderline between these two morphologies ($\phi_B \approx 0.2-0.24$) we found a new morphology designated as the *knitting pattern* (*kp*) morphology. In this morphology, poly(methyl methacrylate) (PMMA) forms peristaltic lamellae in which opposite maxima and minima are spanned by ellipsoidal-shaped cylindrical PEB domains (Figure 1). On the basis of transmission electron microscopy (TEM) results we described this morphology qualitatively and gave a qualitative explanation why this unusual morphology can form.[7]

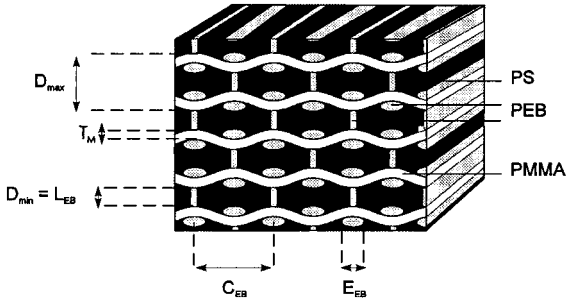

Figure 1. Schematic description of the Knitting Pattern morphology. For the explanations of D_{max}, D_{min}, T_M, L_{EB}, C_{EB}, and E_{EB}, see Table 2.

For AB diblock copolymers only structures have been described in which the interface fulfills the criterion for constant mean curvature (CMC).[8,9] In an ABC triblock copolymer coaxial cylindrical morphology Thomas et al.[5] have shown a slight deviation of this concept and described a structure with weak nonconstant mean curvature. In contrast the interfaces in the knitting pattern morphology exhibit pronounced nonconstant mean curvatures between the various interfaces (H_{AB},

* Author to whom all correspondence should be addressed. Present address: Makromolekulare Chemie II and Bayreuther Institut für Makromolekülforschung, Universität Bayreuth, 95440 Bayreuth, Germany.

† Department of Materials Science and Engineering, Massachusetts Institute of Technology, Cambridge, Massachusetts 02139.

⊗ Abstract published in *Advance ACS Abstracts,* December 15, 1997.

S0024-9297(96)01550-1 CCC: $15.00
Published on Web 01/13/1998

Table 1. Characteristics of SBM/SEBM Triblock Copolymers

polymer	$10^{-3}\ M_n$[a]	M_w/M_n[a]	w_{PS}[b]	ϕ_{PS}	$w_{PB/PEB}$	$\phi_{PB/PEB}$	w_{PMMA}	ϕ_{PMMA}
$S_{35}B_{27}M_{38}{}^{121}$	121	1.06	0.35	0.36	0.27	0.31	0.38	0.33
$S_{35}EB_{27}M_{38}{}^{122}$	122	1.08	0.35	0.36	0.27	0.31	0.38	0.33

[a] $M_i = M_{PS}\phi_i/\phi_{PS}$. M_{PS}, determined by GPC (calibrated with PS). [b] determined from ^{1}H-NMR. w_i, weight fraction of component i; ϕ_i, volume fraction.

H_{BC}, $H_{AC} \neq$ CMC) as well as a variable curvature. Other examples for nonconstant mean curvature structures are the *cylinders at the lamellae* (*lc*), *spheres at lamellae* (*ls*), *cylinder with ring* (*cr*), and the *helical* (*hel*) morphology as reported earlier.[6,10]

In the present paper we will give a detailed structural characterization of the knitting pattern using transmission electron microscopy and small angle X-ray scattering (SAXS).

Experimental Section

Synthesis of SBM and SEBM. The synthesis of the polystyrene-*block*-polybutadiene-*block*-poly(methyl methacrylate) block copolymers (SBM) and polystyrene-*block*-poly(ethylene-*co*-butylene)-*block*-poly(methyl methacrylate) block copolymers (SEBM) was accomplished by sequential anionic polymerization of styrene, butadiene, and methyl methacrylate in tetrahydrofuran in the presence of lithium alkoxides using *sec*-butyllithium as an initiator. Furthermore the center block consisting predominantly of 1,2-units of polybutadiene was hydrogenated, resulting in the corresponding SEBM triblock copolymers. Details are given elsewhere.[11] The characterization of the block copolymers is summarized in Table 1. In our nomenclature $S_uB_vM_w{}^x$, u, v, and w correspond to the weight percent of the components whereas x equals the total molecular weight in kg/mol. For the hydrogenated samples $S_uEB_vM_w{}^x$ the different density of the center block was taken into account. For clarity the labeling of the SEBM samples with respect to their weight fractions corresponds to the original nonhydrogenated triblock copolymers SBM.

Sample Preparation for Transmission Electron Microscopy and Small Angle X-ray Scattering. Transparent 1 mm thick films of the triblock copolymer were slowly cast from $CHCl_3$ and from toluene over a period of 3 weeks. To avoid cross-linking of the nonhydrogenated 1,2-polybutadiene block, further drying and annealing of the block copolymer was performed at room temperature under high vacuum for 2 days. The temperature was then subsequently increased over a period of 6 h up to 185 °C where the samples remained for another 2−6 h. In previous studies no change in morphology has been shown for different annealing conditions, suggesting that the *kp* morphology is a quite stable structure.[6]

Transmission Electron Microscopy. TEM was performed in the bright field mode on a Phillips transmission electron microscope operating at 80 kV and on a JEOL 200 CX transmission electron microscope at 100 kV. Ultrathin sections of the block copolymers were obtained using a Reichert ultramicrotome equipped with a diamond knife. The rigidity of the samples was sufficient to prepare high-quality ultrathin sections at room temperature. The ultrathin sections were stained using gaseous ruthenium tetroxide reacting preferentially with polystyrene (PS) in the SEBM sample or osmium tetroxide reacting preferentially with PB in the SBM sample. RuO_4 was prepared in aqueous solution.

FFT Analysis. Selected regions of TEM prints were digitized at 400 dpi (dots per inch). The image size was 1024 × 1024 pixels and contained about 370 unit cells. A two-dimensional fast Fourier transform (FFT) was then performed to create the image in the reciprocal space.[12] Subsequent Fourier indexing of the transformed image permitted determination of the unit cell and its space group.

Small Angle X-ray Scattering. The X-ray diffraction (SAXS) data were acquired at room temperature on the Time-Resolved Diffraction Facility (station X12B) at the National Synchrotron Light Source at Brookhaven National Laboratory using a custom-built two-dimensional gas delay detector (10 × 10 cm^2, 512 × 512 pixels), interfaced to a real-time histogramming memory system.[13] The optical system provides a doubly-focused (spot size, 0.5 × 0.5 mm^2 filled width at half-maximum) monochromatic X-ray beam (bandpass, $\sim 5 \times 10^{-4}$ $\Delta\lambda/\lambda$) spanning 0.9−1.5 Å (here $\lambda = 1.38$ Å was chosen). Since all the patterns were circularly symmetric around the main beam, the frames were azimuthally integrated about the beam center in bins of 1 pixel width. The q conversion was determined by dividing the width of each pixel (105 μm) by the sample-to-detector distance (1.86 m).

Analysis of the X-ray Data. Scattering data are represented in the form of intensity measurements as a function of the scattering vector q defined by

$$q = \frac{4\pi \sin\theta}{\lambda} \tag{1}$$

where λ is the wavelength of the X-ray and θ is half of the scattering angle defined as 2θ. Using Bragg's equation

$$\lambda = 2d_{hkl} \sin\theta \tag{2}$$

and (1) the d-spacing of the reflection hkl is given by

$$d_{hkl} = \frac{2\pi}{q_{hkl}} \tag{3}$$

For the allowed reflections of a lamellar structure, the ratios q_{n00}/q_{100} equal 1, 2, 3, ... For a lamellar structure the repeat spacing is most accurately obtained by plotting the d-spacing of the various reflections d_{n00} versus the reciprocal value of the order of reflections, $1/n$.

Results and Discussion

The formation of morphologies in the SBM and SEBM systems is governed by the relatively weak incompatibilities of the PS and PMMA end blocks compared to the strong incompatibility of the polybutadiene (PB) or poly(ethylene-co-butylene) midblock to the PS and PMMA end blocks, respectively ($\gamma_{SM} \ll \gamma_{SB}$; $\gamma_{SEB} < \gamma_{BM}$; γ_{EBM}). Furthermore, hydrogenation of the center block is associated with an increase of the unfavorable interactions between the center block PEB and the PS and PMMA end blocks.

Investigation of the Nonhydrogenated Sample $S_{35}B_{27}M_{38}{}^{121}$. A transmission electron micrograph of sample $S_{35}B_{27}M_{38}{}^{121}$ cast from chloroform and stained with OsO_4 is shown in Figure 2.

As might be expected for an almost symmetric block copolymer system with respect to its composition, a lamellar morphology is formed. Due to the applied staining conditions PB appears dark, PS appears as the thicker gray layer, and PMMA is the somewhat thinner and lighter gray layer due to the mass loss from electron beam damage. The lamellar repeat unit as obtained from TEM (... ABCB ...) is approximately 46 nm ($l_{PS} \approx$ 18 nm; $l_{PB} \approx 9$ nm; $l_{PMMA} \approx 11$ nm; where l_i is the thickness of a layer formed by component i). It can be recognized that the PMMA microphase has lost about one-half of its expected thickness due to beam damage. In the case of PS and PMMA, bilayer domains are

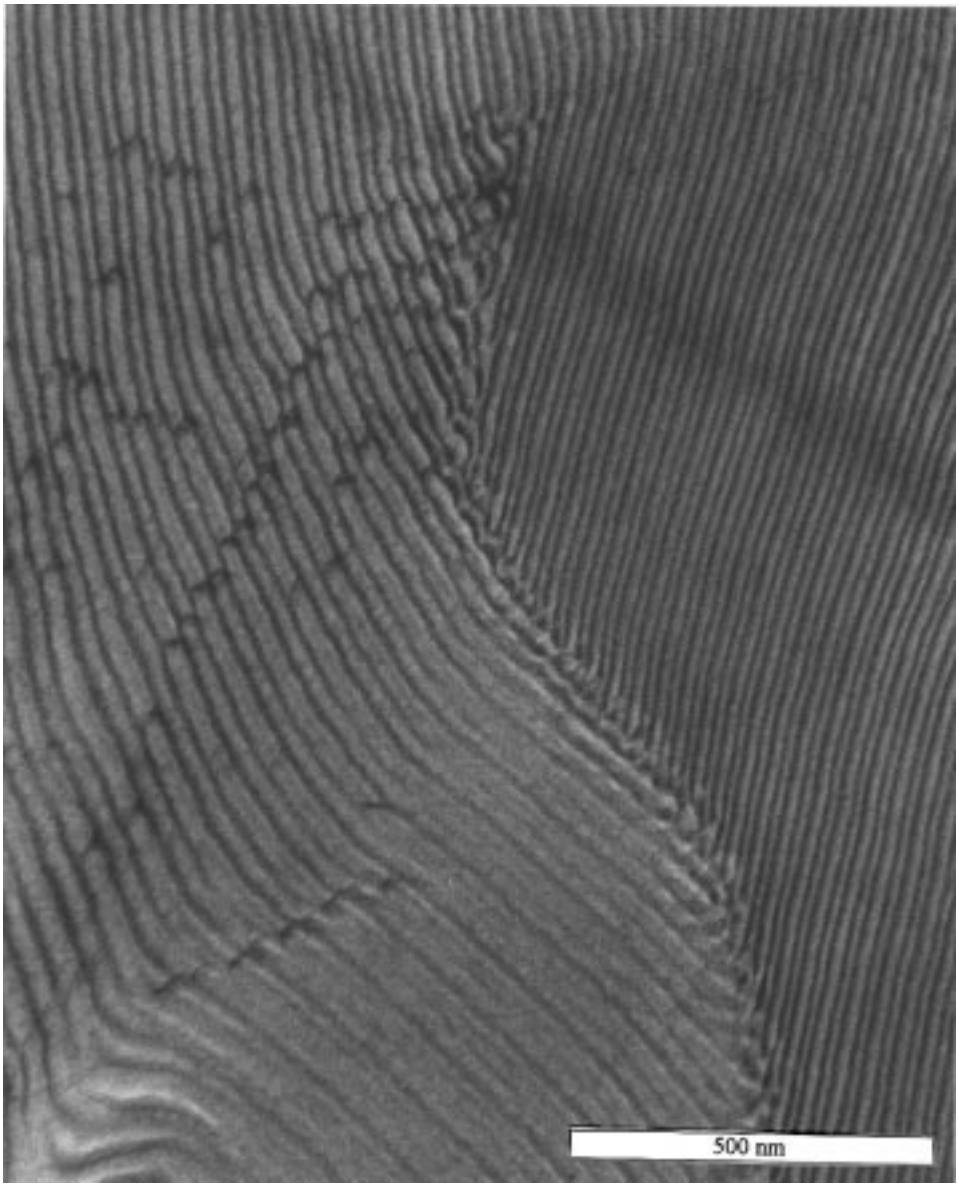

Figure 2. Bright field transmission electron micrograph of $S_{35}B_{27}M_{38}^{121}$ stained with OsO_4 and cast from chloroform.

formed, a single-bridged midblock layer is formed in the case of PB. At the high magnification a slight modulation of the PB layer thickness is recognizable (waviness parallel to the lamella). No regular distance between these modulations can be determined. This modulation of the A/B and B/C intermaterial dividing surfaces is perhaps indicative of a pretransitional fluctuation for the formation of cylinders at the A/C interface.[6,7] This is also indicated by the dark breaks in the PS and PMMA layers. The same lamellar morphology has been obtained in toluene cast films.

The semilogarithmic SAXS profile (Figure 3) of sample $S_{35}B_{27}M_{38}^{121}$ exhibits three strong and narrow peaks at low q values ($q < 3 \times 10^{-3}$) as well as four broader and weaker peaks at higher q. Calculating the ratios q_{n00}/q_{100} reveals ratios corresponding to a lamellar system (1.0:2.0:4.04:5.04:7.08:8.08:10.09) up to the 10th order of reflections. The reflections corresponding to [300], [600], and [900] are missing. The d-spacing for the lamellar repeating unit is calculated as 83 nm from both the first peak and from a plot q_{n00} versus $1/n$.

A huge difference in the dimensions for the lamellar repeating unit was found by TEM (46 nm) and SAXS

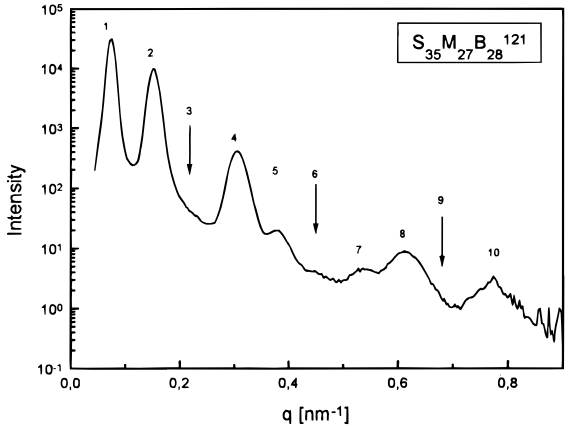

Figure 3. Semilogarithmic plot of the scattered intensity versus the scattering vector q for the specimen $S_{35}B_{27}M_{38}^{121}$ with lamellar morphology. The arrows indicate the positions of missing reflections q_{300}, q_{600}, and q_{900}, the numbers the order of reflection.

(83 nm). Calculating the dimensions of the PS, PB, and PMMA layers on the basis of the domain spacing obtained by SAXS and the volume fraction of the

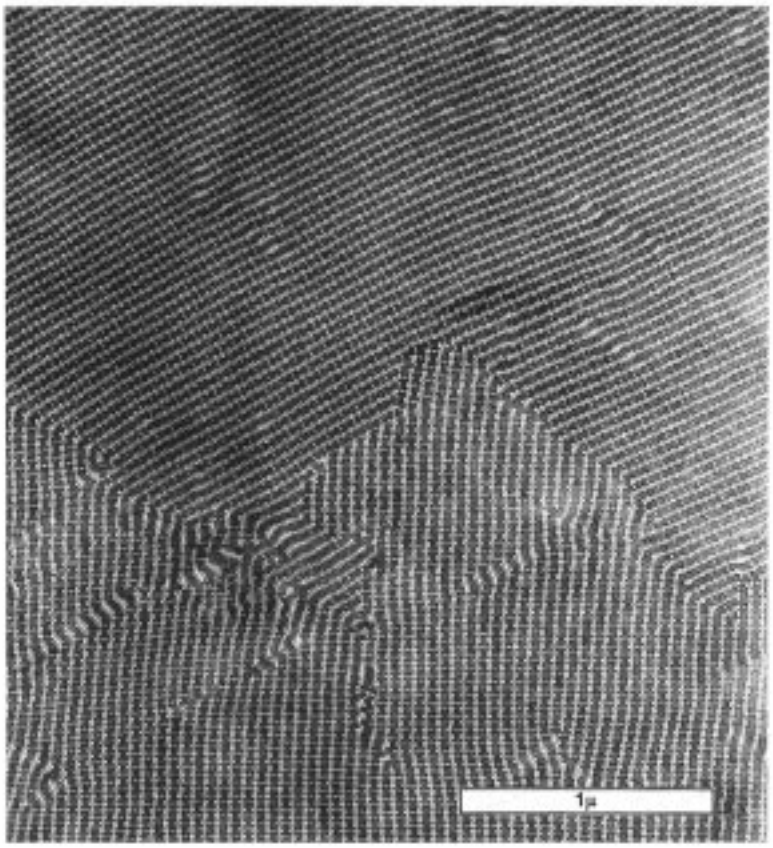

(a)

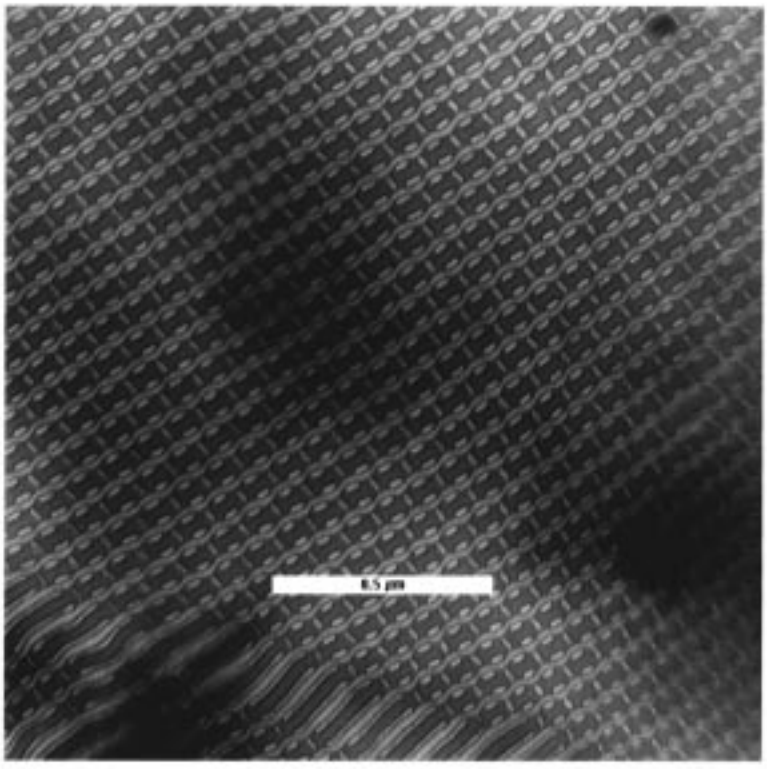

(b)

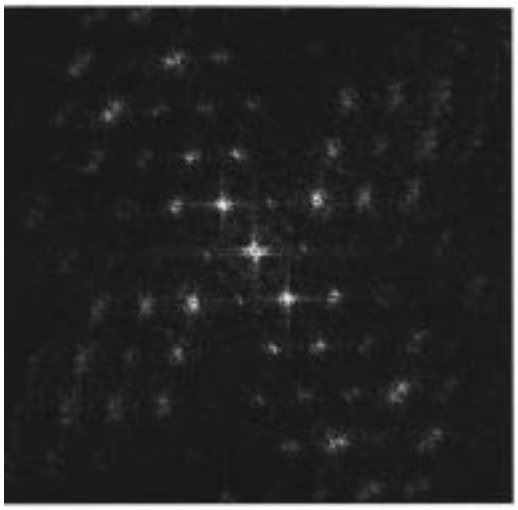

(c)

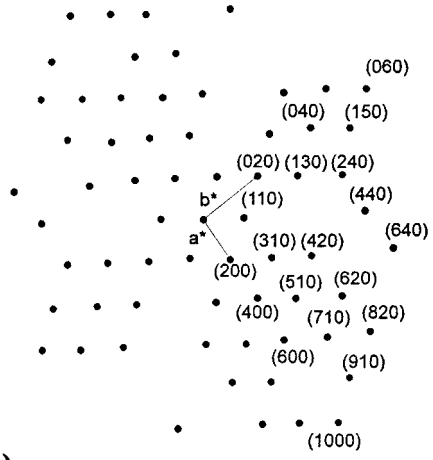

(d)

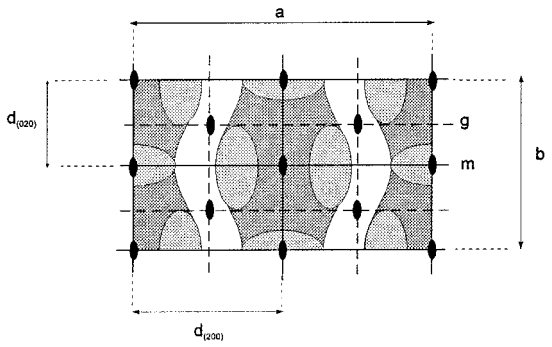

(e)

Figure 4. (a) Bright field transmission electron micrograph of $S_{35}EB_{27}M_{38}^{122}$ stained with RuO_4. (b) Bright field transmission electron micrograph of $S_{35}EB_{27}M_{38}^{122}$ stained with RuO_4 at higher magnification. (c) FFT image of the *kp* morphology. (d) Indexed FFT pattern. **a***, **b*** correspond to the lattice parameters of the unit cell in the reciprocal space. (e) Schematic description of the unit cell in the knitting pattern morphology. Included are the locations of the symmetry elements of the two-dimensional plane group *c*2*mm*: mirror planes (m, black lines), glide planes (g, dotted lines), c2 axes (black ellipsoidal objects). **a** and **b** correspond to the lattice parameters of the unit cell (**a** > **b**).

Table 2. Characteristic Dimensions of the Knitting Pattern Morphology[a]

T_M [nm]	D_{max} [nm]	$D_{min} = L_{EB}$ [nm]	E_{EB} [nm]	C_{EB} [nm] = b	a [nm]
13.0 ± 1	69.4 ± 3	30.2 ± 2	12.8 ± 2	63.1 ± 4	100.1 ± 4

[a] T_M: thickness of the PMMA lamellae. D_{max}: distance between concave parts of the PMMA lamellae corresponding to the largest distance. D_{min}: distance between convex parts of the PMMA lamellae corresponding to the smallest distance as well as the diameter of the PEB connectors along the long half axes, L_{EB}; E_{EB}: diameter of the PEB connectors along the small half axes. C_{EB}: distance of the centers of PEB connectors, absolute value of the lattice parameter **b** of the unit cell. **a**: absolute value of the lattice parameter **a** of the unit cell.

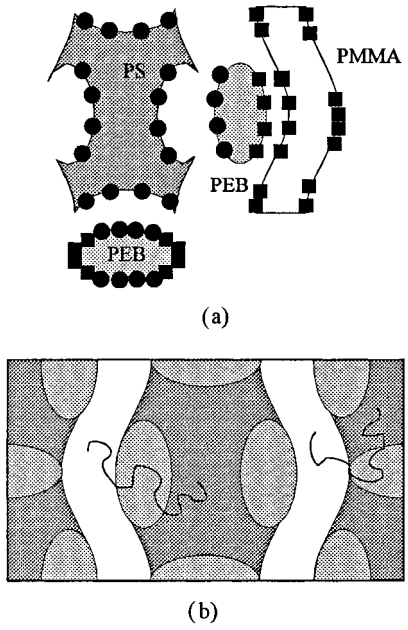

Figure 5. (a) Schematic description of the junction distribution along the intermaterial dividing surface. ●, PS/PEB junctions; ■, PEB/PMMA junctions. (b) Schematic description of the chain conformation within the unit cell.

sample, the following dimensions should result: $l_{PS(calc)} \approx 30$ nm; $l_{PB(calc)} \approx 13$ nm; $l_{PMMA(calc)} \approx 27$ nm. These dimensions do not agree with electron microscopic dimensions of the layer thickness. These observations can be attributed to the severe beam damage of the PMMA and some additional damage in the PS and/or PB microdomains. On the basis of tilting experiments the given TEM spacing is the largest that can be detected.

Investigation of the Hydrogenated Sample $S_{35}EB_{27}M_{38}$[122]. For the hydrogenated sample $S_{35}EB_{27}M_{38}$[122] we have recently reported the formation of the knitting pattern *kp* morphology.[7] Figure 4a shows a bright field transmission electron micrograph of this morphology stained with RuO_4 of a sample cast from $CHCl_3$.

Due to the staining conditions, PS appears dark whereas PMMA, forming a undulating (peristaltic) lamellar structure, appears bright. The PEB domains connect the PMMA domains and form additional ellipsoidal-shaped domains which are weakly stained and appear light gray. The PEB phase boundary appears dark due to the preferred staining of the interface in this system.[14,15] The dimensions of this morphology obtained from TEM are summarized in Table 2; a schematic description is given in Figure 1.

Table 3. Dimensions and Ratios of the Lattice Parameters Obtained from SAXS and TEM

lattice parameter **a**		lattice parameter **b**		ratio of the lattice parameters **a**/**b**	
$\mathbf{a}_{TEM}$	100	$\mathbf{b}_{TEM}$	63	$(\mathbf{a}/\mathbf{b})_{TEM}$	1.6
$\mathbf{a}_{SAXS}$	153	$\mathbf{b}_{SAXS}$	87	$(\mathbf{a}/\mathbf{b})_{SAXS}$	1.75
$\mathbf{a}_{TEM}/\mathbf{a}_{SAXS}$	0.65	$\mathbf{b}_{TEM}/\mathbf{b}_{SAXS}$	0.72		

Figure 4b exhibits a well-ordered region of the knitting pattern corresponding to a view normal to the plane containing **a** and **b** (i.e., [001]). A FFT analysis of a similar highly ordered region (Figure 4c) consisting of approximately 14 × 27 cells allows the determination of the two-dimensional space group in this sample. The indexed (*hk*0) pattern along the (001) direction is shown in Figure 4d.

Reflections can be identified up to the 6th order corresponding to the high order exhibited in TEM. From this analysis, the two-dimensional plane symmetry group can be determined as *c*2*mm* fulfilling the condition $h + k = 2n$ for allowed reflections. The structure of the corresponding orthorhombic unit cell exhibiting mirror planes, glide planes, and two-fold axes is schematically shown in Figure 4e.

Subdividing the unit cell into the areas belonging to the phases of the three components the shapes of these regions are very remarkable (Figure 5a). For polystyrene the phase exhibits a large variation in thickness along both axes, resulting in a further constraint of the chains. Furthermore since A and C (PS and PMMA) are not directly linked together, an inhomogenous distribution of the A/B and B/C junctions along the intermaterial dividing surface indicated in Figure 5a exists.

The shape of the A/B intermaterial dividing surface exhibits a highly nonconstant mean curvature which even changes sign. For component B two different kinds of PEB domains are found: the ellipsoidal-shaped PEB domains parallel to the wavy PMMA lamellae and the oblong-shaped PEB connectors oriented perpendicular to the PMMA lamellae, at the smallest spacing between adjacent lamellae. In contrast to component A, the B domains possess a more regular shape. The junctions between the center block B and the end blocks A (A/B) and C (B/C), respectively, are distributed along the entire interface: the B/C junctions are placed on the smaller side of the connectors while the A/B junctions are located on the longer side of the connector. Since the interfacial tension between the center block PEB and PS is lower than that between the center block and PMMA, less PEB/PMMA interface will be created. The ellipsoidal-shaped PEB domains are distributed on either side of the PMMA domains. The PMMA lamellae are sinusoidal and also posses a nonconstant mean curvature intermaterial dividing surface for which the mean curvature also changes sign. The B/C junctions are preferentially located at regions of high interfacial curvature. Within the unit cell, two different classes of chain conformation (Figure 5b) exist, which is due to the presence of two different types of PEB domains.

The semilogarithmic SAXS profile of the *kp* is shown in Figure 5, exhibiting two broad and strong peaks at low values of q as well as four weak reflections at higher values of q. The calculated ratios q_n/q_1 are in 1.0, 1.77, 2.51, 3.54, 4.15, and 5.26. No "classical" block copolymer morphology shows this sequence of SAXS maxima. For the interpretation of this profile the information obtained by determining the two-dimensional symmetry

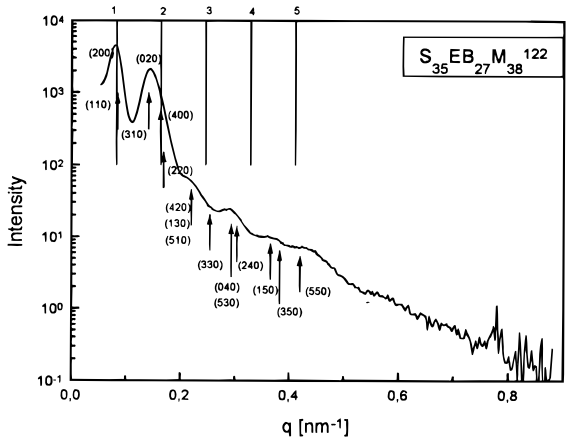

Figure 6. Semilogarithmic plot of the scattered intensity versus the scattering vector **q** for the specimen $S_{35}EB_{27}M_{38}^{122}$ cast from $CHCl_3$. The arrows indicate the calculated allowed reflections up to the 5th order on the basis of the *c*2*mm* symmetry group. The first peak is chosen as the (200) and the second peak as the (020) reflection. The arrows and numbers indicate the positions of the allowed reflections from the *c*2*mm* structure. The vertical lines represent the calculated positions expected for a lamellar morphology on the basis of the first peak.

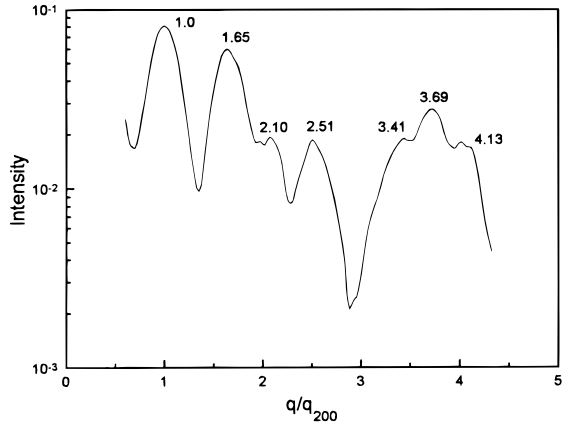

Figure 7. Circular averaged intensity of the FFT pattern versus the ratio q_n/q_{200}.

group can be used. For the *c*2*mm* space group only reflections fulfilling the condition $h + k = 2n$ are allowed and thus may be found in the SAXS pattern. The first allowed reflections are thus (110), (200), (020), (220), (310), (130), and (330). Using

$$\frac{1}{d_{hk0}^2} = \frac{h^2}{\mathbf{a}^2} + \frac{k^2}{\mathbf{b}^2} \tag{4}$$

With **a** and **b** (**a** > **b**) corresponding to the sides of a rectangular unit cell one can establish relations between certain reflections and *d*-spacings. Identifying the first two peaks with any of the allowed reflections results in values of **a** and **b**. The remaining scattering maxima in the profile must agree with the calculated positions of allowed reflections, although one has to consider that peaks might be missing due to a very large *d*-spacing or from cancellations by the form factor due to overlapping with neighboring peaks. Using this method and identifying the first two peaks as reflections resulting from (200) and (020) planes, respectively, the absolute values of the vectors of the unit cell **a** and **b** are calculated as 153 and 86 nm (Table 3). With these the

Figure 8. Bright field transmission electron micrograph of $S_{35}EB_{27}M_{38}^{122}$ cast from toluene and stained with RuO_4.

positions for the remaining allowed reflections ($h + k = 2n$) can be calculated up to the 5th order (Figure 6). Most of expected reflections are very close together, causing the observed broad scattering maxima (i.e., second and third peak). Due to the differences in electron densities, which is largest between PMMA and PEB, scattering can occur from any of these objects, resulting in a complicated intensity pattern, which has not been evaluated.

The lattice parameters **a** and **b** can be assigned to characteristic distances within the morphology: **a** is the distance between two PEB connectors perpendicular to the PMMA lamellae (Figure 4e). The distance **b** describes the distance C_{EB}. The dimensions of the unit cell obtained by SAXS show larger values than the dimensions obtained by TEM. Calculating the ratio **a**/**b** for SAXS and TEM results in 1.75 and 1.6, respectively (Table 3). These different ratios are due to a more pronounced shrinking along the (200) than along the (020) direction.

Performing a circular average of the intensity in the FFT pattern allows a comparison between data obtained from SAXS and TEM. Figure 7 shows the circular averaged intensity versus the ratio of q/q_{200} whereas q_{200} refers to the scattering vector of the first peak. In the profile, seven peaks can be identified at positions $q_n/q_{200} = 1.0$, 1.65, 2.10, 2.51, 3.41, 3.69, and 4.13. These values match the ratios obtained from the SAXS pattern of the $S_{35}EB_{27}M_{38}^{122}$ sample. The slight deviation is due to the shrinkage of the sample in the electron beam which is reflected in the TEM image and thus in the FFT pattern and the values of the lattice parameters **a** and **b**. Multiplying the unit cell vectors in the

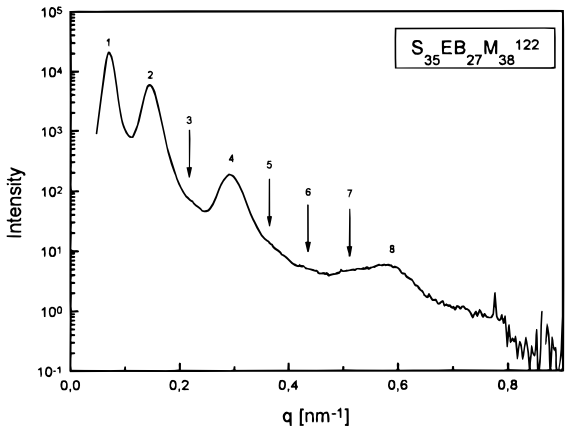

Figure 9. Semilogarithmic plot of the scattered intensity versus the scattering vector q for the specimen $S_{35}EB_{27}M_{38}^{122}$ cast from toluene, exhibiting a lamellar morphology. The arrows indicate the positions of missing reflections q_{300}, q_{500}, q_{600}, and q_{700}.

reciprocal lattice of the FFT pattern by the reciprocal value of the shrinkage, the radial average will be even more comparable to the SAXS profile.

A change in morphology is observed when the hydrogenated sample is cast from toluene. The TEM micrograph of this sample stained with RuO_4 exhibits a poorly ordered lamellar morphology with ... S(EB)M(EB) ... as the repeating unit. Some defect structures are similar to structural elements found in the knitting pattern morphology (Figure 8).

The SAXS profile of this sample shows four strong peaks which agree with a lamellar structure with q_n/q_1 ratios which equal 1.0, 2.0, 4.0, and 7.9. The 3, 5, 6, and 7 reflections are missing or are very weak (Figure 9). From the first reflection the *d*-spacing is calculated as 88 nm, plotting q_{n00} versus $1/n$ with n as the order of refection revealing the same value. The TEM *d*-spacing is measured as 65 nm. This discrepancy is likely due to beam damage of the PMMA layer as mentioned earlier. Since Figure 3 also corresponds to a lamellar morphology of nearly the same ϕ_A, ϕ_B, and ϕ_C one expects the two patterns (Figures 3 and 9) to look quite similar. This is indeed the case; however, Figure 9 suggests a poor order in agreement with TEM observations.

By using toluene instead of $CHCl_3$ as the casting solvent, a lamellar morphology is formed by $S_{35}EB_{27}M_{38}^{122}$ despite the same annealing conditions. Toluene is a better solvent for the center block PEB (δ_{PEB} 7.85 (cal/cm^3)^2 (lit.[16]); δ_{CHCl3} 9.3 (cal/cm^3)^2; $\delta_{toluene}$ 8.3 (cal/cm^3)^2 (lit.[17]). For this reason the PEB block remains in solution longer whereas in the case of $CHCl_3$ the PEB microdomains are formed first, resulting in individual domains with large positive interfacial curvature. This influence of the solvent on the center block on the morphology of this sample reveals the close position of this material with respect to the borderline between the *ll* and the *lc* morphologies.

Conclusions

The knitting pattern structure represents the second sample of a block copolymer where hydrogenation results in a fundamental change of the microphase morphology. A similar transition has been observed upon hydrogenation of a SBM triblock copolymer forming a *ls* morphology (B spheres located at the A/C interface).

The new *kp* morphology has been studied by TEM, FFT, and SAXS, allowing a more complete characterization of the structure. FFT of bright field images permit the determination of the two-dimensional space group to be *c*2*mm*. The complex SAXS pattern can be well fit on the basis of the *c*2*mm* structure. This SEBM sample of a block copolymer possesses a two-dimensional structure with centered rectangular symmetry. The intermaterial dividing surfaces in this triblock have highly nonconstant mean curvatures due to the nonuniform distribution of the A/B and B/C junctions. Casting this sample from toluene instead of $CHCl_3$ results in a lamellar structure due to the differences in solubility of the centered EB block.

Acknowledgment. This work was supported by the Bundesminister für Forschung und Technologie and by the BASF AG through joint project 03M40861. Additional support was from the Deutsche Forschungsgemeinschaft through SFB 262 project S-14, the Graduierten Kolleg, and from the National Science Foundation, Division of Materials Research, through project DMR 92-14853. The authors are indebted to Mr. Würfel (Institut für Physikalische Chemie, Mainz) for his kind assistance during the electron microscopic measurements. U.B. is grateful to C. Honeker (MIT) and M. Capel (Brookhaven) for running the SAXS experiments at Brookhaven and J. Chen for helpful discussions during her visit in E. L. Thomas' research group.

(1) Molau, G. E. In *Colloidal and Morphological Behaviour of Block Copolymers*; Molau, G. E., Ed.; Plenum Press: New York, 1971.
(2) Riess, G. In *Thermoplastic Elastomers. A Comprehensive Review*; Ledge, N. R., Holden, G., Schroeder, H. E., Eds.; Hanser: Munich, 1987; Chapter 12.2, p 325.
(3) Hadjuk, D. A.; Harper. P. E.; Gruner, S. M.; Honeker, C. C.; Kim, G.; Thomas, E. L.; Fetters, L. J. *Macromolecules* **1994**, *27*, 4063.
(4) Mogi, Y.; Mori, K.; Kotsuji, H.; Matsushita, Y.; Noda, I.; Han, C. *Macromolecules* **1993**, *26*, 2636.
(5) Gido, S. P.; Schwark, D. W.; Thomas, E. L.; Goncalves, M. C. *Macromolecules* **1993**, *26*, 2636.
(6) Stadler, R.; Auschra, C.; Beckmann, J.; Krappe, U.; Voigt-Martin, I. V.; Leibler, L. *Macromolecules* **1995**, *28*, 3080.
(7) Breiner, U.; Krappe, U.; Stadler, R. *Macromol. Rapid Commun.* **1996**, *17*, 567.
(8) Hashimoto, T.; Koizumi, S.; Hasegawa, H.; Izumitani, T.; Hyde, S. T. *Macromolecules* **1992**, *25*, 1433.
(9) Thomas, E. L.; Anderson, D. M.; Henkee, C. S.; Hoffman, D. *Nature* **1988**, *334*, 598.
(10) Krappe, U.; Stadler, R.; Voigt-Martin, I.-G. *Macromolecules* **1995**, *28*, 4458.
(11) The synthesis followed the procedure given in Auschra, C.; Stadler, R. *Polym. Bull.* **1993**, *26*, 2171.
(12) Gonzales, R. C.; Wintz, P. *Digital Image Processing*; Addison-Wesley: Reading, MA, 1977.
(13) Capel, M. S.; Smith, G. V.; Yu, B. *Rev. Sci. Instrum.* **1995**, *66*, 2295.
(14) Auschra, C.; Stadler, R. *Macromolecules* **1993**, *26*, 2171.
(15) Auschra, C.; Stadler, R. *Macromolecules* **1993**, *26*, 6364.
(16) Schuster, R. *Angew. Makromol. Chem.* **1992**, *202*, 159.
(17) Wu, S. In *Polymer Handbook*, 3rd ed.; Brandrup, J., Immergut, E. H., Eds.; J. Wiley & Sons: New York, 1989; Chapter VI, p 411.

MA961550D